Nanoscale optical field localization by resonantly focused plasmons

Liang Feng,[1,*] Derek Van Orden,[2] Maxim Abashin,[1] Qian-Jin Wang,[3] Yan-Feng Chen,[3] Vitaliy Lomakin,[1] and Yeshaiahu Fainman[1]

[1]*Department of Electrical and Computer Engineering, University of California, San Diego, La Jolla, CA 92093, USA*
[2]*Department of Physics, University of California, San Diego, La Jolla, CA 92093, USA*
[3]*National Laboratory of Solid State Microstructures, Nanjing University, Nanjing, Jiangsu 210093, People's Republic of China*
[*]*Corresponding author: lifeng@ucsd.edu*

Abstract: We experimentally demonstrate use of plasmonic resonant phenomena combined with strong field localization to enhance efficiency of confining optical fields in a Si waveguide. Our approach utilizes a plasmonic resonant nano-focusing-antenna (RNFA), that simultaneously supports several focusing mechanisms in a single nanostructure, integrated with a lossless Si waveguide utilized with silicon-on-insulator (SOI) technology, to achieve a sub-diffraction limited focusing with a nanoscale (deeply subwavelength) spot size. The metallic RNFA effectively converts an incoming propagating waveguide mode to a localized resonant plasmon mode in an ultrasmall volume in all 3 dimensions. The near-field optical measurements of the fabricated RNFA using heterodyne near-field scanning optical microscope (H-NSOM) validate the theoretical predictions showing strong optical field localization.

OCIS codes: (250.5403) Plasmonics; (240.6680) Surface plasmons; (130.3120) Integrated optical devices.

References and links

1. H. Raether, *Surface Plasmons on Smooth and Rough Surfaces and on Gratings* (Springer, Berlin, 1998).
2. W. L. Barnes, A. Dereux, and T. W. Ebbesen, "Surface plasmon subwavelength optics," Nature **424,** 824-830 (2003).
3. E. Ozbay, "Plasmonics: merging photonics and electronics at nanoscale dimensions," Science **315**, 189-193 (2006).
4. Z. Liu, H. Lee, C. Sun, and X. Zhang, "Far-field optical hyperlens magnifying sub-diffraction-limited objectS," Science **315**, 1686 (2007).
5. N. Fang, H. Lee, C. Sun, and X. Zhang, "Sub-diffraction-limited optical imaging with a silver superlens," Science **308**, 534-547 (2005).
6. L. Pang, G. Hwang, B. Slutsky, and Y. Fainman "Spectral sensitivity of two-dimensional nanohole array surface plasmon polariton resonance sensor," Appl. Phys. Lett. **91,** 123112 (2007).
7. W. A. Challener, T. W. McDaniel, C. D. Mihalcea, K. R. Mountfield, K. Pelhos, and I. K. Sendur, "Light delivery techniques for heat-assisted magnetic recording," Jpn. J. Appl. Phys. **42,** 981-988 (2003).
8. R. Hooper, T. W. Preist, and J. R. Sambles, "Making tunnel barriers (including metals) transparent," Phys. Rev. Lett. **97,** 053902 (2006).
9. Z. Liu, J. M. Steele, W. Srituravanich, Y. Pikus, C. Sun, and X. Zhang, "Focusing surface plasmons with a plasmonic lens," Nano Lett. **5,** 1726-1729 (2005).
10. L. Yin, V. K. Vlasko-Vlasov, J. Pearson, J. M. Hiller, J. Hua, U. Welp, D. E. Brown, and C. W. Kimball, "Subwavelength focusing and guiding of surface plasmons," Nano Lett. **5,** 1399-1402 (2005).
11. A. Hohenau, J. R. Krenn, A. L. Stepanov, A. Drezet, H. Ditlbacher, B. Steinberger, A. Leitner, and F. R. Aussenegg, " Dielectric optical elements for surface plasmons," Opt. Lett. **30,** 893-895 (2005).
12. R. Rokitski, K. A. Tetz, and Y. Fainman, "Propagation of femtosecond surface plasmon polariton pulses on the surface of a nanostructured metallic film: space-time complex amplitude characterization," Phys. Rev. Lett. **95,** 177401 (2005).
13. L. Feng, K. A. Tetz, B. Slutsky, V. Lomakin, and Y. Fainman, "Fourier plasmonics: diffractive focusing of in-plane surface plasmon polariton waves," Appl. Phys. Lett. **91,** 081101 (2007).

#107134 - $15.00 USD Received 3 Feb 2009; revised 3 Mar 2009; accepted 9 Mar 2009; published 11 Mar 2009

14. M. I. Stockman, "Nanofocusing of optical energy in tapered plasmonic waveguides," Phys. Rev. Lett. **93,** 137404 (2004).
15. E. Moreno, S. G. Rodrigo, S. I. Bozhevolnyi, L. Martin-Moreno, and F. J. Garcia-Vidal, "Guiding and focusing of electromagnetic fields with wedge plasmon polaritions," Phys. Rev. Lett. **100,** 023901 (2008).
16. D. K. Gramotnev, D. F. P. Pile, M. W. Vogel, and X. Zhang, "Local electric field enhancement during nanofocusing of plasmons by a tapered gap," Phys. Rev. B **75,** 035431 (2007).
17. E. Verhagen, L. Kuipers, and A. Polman, "Enhanced nonlinear optical effects with a tapered plasmonic waveguide," Nano Lett. **7,** 334-337 (2007).
18. C. Ropers, C. C. Neacsu, T. Elsaesser, M. Albrecht, M. B. Raschke, and C. Lienau, " Grating-coupling of surface plasmons onto metallic tips: a nanoconfined light source," Nano Lett. **7,** 2784-2788 (2007).
19. E. Hutter and J. H. Fendler, "Exploitation of localized surface plasmon resonance," Adv. Mater. **16,** 1685-1706 (2004)..
20. C. Langhammer, M. Schwind, B. Kasemo, and I. Zoric, "Localized surface plasmon resonances in aluminum nanodisks," Nano Lett. **8,** 1461-1471 (2008).
21. Y. Lu, G. L. Liu, J. Kim, Y. X. Mejia, and L. P. Lee, "Nanophotonic crescent moon structures with sharp edge for ultrasenstive biomolecular detection by local electromagnetic field enhancement effect," Nano Lett. **5,** 119-124 (2005).
22. M. Cinchetti, A. Gloskovskii, S. A. Nepjiko, G. Schonhense, H. Rochholz, and M. Kreiter, "Photoemission electron microscopy as a tool for the investigation of optical near fields," Phys. Rev. Lett. **95,** 047601 (2005).
23. A. Sundaramurthy, P. J. Schuck, N. R. Conley, D. P. Fromm, G. S. Kino, and W. E. Moerner, "Toward nanometer-scale optical photolithography: utilizing the near-field of bowtie optical nanoantennas," Nano Lett. **6,** 355-360 (2006).
24. P. Muhlschlegel, H.-J. Eisler, O. J. F. Martin, B. Hecht, and D. W. Pohl, "Resonant optical antennas," Science **308,** 1607-1609 (2005).
25. R A. Alu and N. Engheta, "Input impedance, nanocircuit loading, and radiation tuning of optical nanoantennas," Phys. Rev. Lett. **101**, 043901 (2008).
26. A. Nesci, and Y. Fainman, "Complex amplitude of an ultrashort pulse with femtosecond resolution in a waveguide using a coherent NSOM at 1550 nm," Proc. SPIE **5181,** 62-69 (2003).
27. A. Gelman, J. B. Carlin, H. S. Stern, and D. B. Rubin, *Bayesian Data Analysis* (Chapman & Hall/CRC, 2004).

1. Introduction

Nanoscale field confinement enabled by plasmonic phenonena [1] has great potential to revolutionize many applications in nanophotonics, including bio-sensing, imaging, and magnetic recording [2-7]. Many metals in the optical frequency regime behave as electron plasmas, which below the plasma resonance frequency are characterized by a negative (real part of) permittivity. This property is equivalent to having a positive quantum mechanical potential as opposed to negative potential corresponding to dielectric materials [8]. Metal-dielectric surfaces can thus support SPPs, which are electromagnetic modes, extending evanescent fields from both sides of the interface [1]. Various schemes using propagating surface plasmon polariton (SPP) waves have been suggested [9-13]. For properly chosen parameters, the effective index of the SPP modes can be considerably higher than the index of the surrounding dielectric media. The thin metallic structures can support high effective index anti-symmetric (short-range) SPP modes and thus strong field localization [14-18]. However, this is achieved on the expense of an intrinsically high power loss associated with SPP propagation in such high effective index structures, restricting their practical applications. Localized surface plasmons (LSPs), which are associated with collective oscillations of free electrons in a metal particle [1, 19-22], are arguably a better sub-diffraction limited focusing alternative to adiabatic SPPs due to their smaller domain of confinement. Additional ultra-strong confinement can be achieved using transverse electromagnetic (TEM) fields supported by small gaps between metals [23-25].

2. Geometry of resonant nano-focusing-antenna

It is highly desired to have an optical nanostructure that can simultaneously support all focusing mechanisms that we describe above and thus produce a single nano-focusing spot with strong field localization. In this letter, we introduce a novel plasmonic resonant nano-focusing-antenna (RNFA) geometry for efficient field nano-focusing and localization that

#107134 - $15.00 USD Received 3 Feb 2009; revised 3 Mar 2009; accepted 9 Mar 2009; published 11 Mar 2009

simultaneously uses three physical mechanisms: LSPs [19], thin metallic wedge localization of SPP with high effective index [14-18], and TEM field localization [23-25] (see Fig. 1). We fabricate the RNFA nanostructure and for the first time experimentally demonstrate sub-diffraction limited focusing with a nanoscale (deeply subwavelength) spot size. The LSPs, thin metallic wedge localization, and TEM field localization in RNFA provide ultra-high confinement (on the order of 25 nm), while simultaneously allowing increasing the overall efficiency of the localized fields due to the resonant nature of LSP and associated large stored near-field energy.

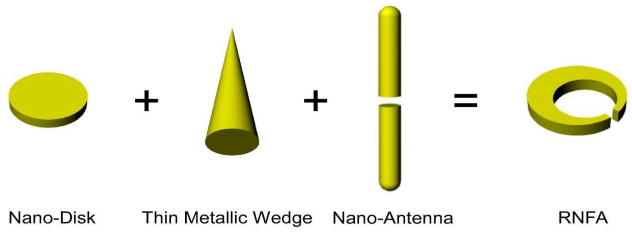

Fig. 1. The proposed novel RNFA nanostructure allows simultaneously achieving three optical field localization mechanisms realized with plasmonic phenomena using the corresponding realization geometries: resonant LSPs in nano-disks, thin metallic wedge localization of SPP fields, and TEM field localization in nano-antennas.

LSPs are special electromagnetic eigen modes associated with free electron longitudinal vibrations, exhibiting resonant singularity in spectra such as Mie resonances for small metallic spheres. LSPs on the nano-disk are associated with vibrating electrons on the disk sidewall and they follow the Born-von-Kármárn periodic boundary condition for LSPs that requires that an electron must oscillate in phase after the plasmon wave has experienced an entire round loop. While LSPs on the nano-disk structure already lead to strong field confinement, a significantly smaller field localization spot size can be achieved by introducing the field edge localization by sharpening the nanodisk. The effective index near the sharp edge can be very high (corresponding to a very low potential) thereby resulting in strong plasmonic field localization. The plasmonic fields on two sharp thin metallic wedges of the RNFA in Fig. 1 are strongly coupled and they support nearly uniformly distributed TEM type fields regardless of the gap size. These TEM fields are similar to the strong fields obtained at the feed points or small air gaps in dipole, bow-tie, and other small antennas. The gap operates as a capacitor that is known to confine strong fields even in the static regime. Such a nano-capacitor strongly confines the plasmonic fields, already enhanced due to the LSP and the sharp thin metallic wedge localizations.

It should be noticed that though our RNFA geometry looks, in the general shape, similar to the nano-crescent-moon that has been investigated [21, 22], the physics behind our structure is quite different. In all prior work, two edges of the nano-crescent-moon are independent. This discontinuity in the structure actually destroys the continuity of the excited plasmon mode. As a result, the localized surface plasmon resonance in the nano-disk, which is continuous in both structure and plasmon wave mode, *can not be reproduced by their nano-crescent-moon*. Their nano-crescent-moon is only in the level of the deformation of conventional taper focusing structures (like Refs. 14-18). Our novel contribution introduces the idea of a dipole wire antenna from microwaves to overcome the issue of the structure discontinuity, and perfectly reproduced the localized surface plasmon resonance in the nano-disk (see Fig. 4), thereby simultaneously realizing 3 localization mechanisms. As we mentioned above, the novel focusing effect is drastically enhanced by coexistence of all 3 localizations (the performance can be degraded drastically if one of them is missing). For instance, the intensity of the focusing spot in our RNFA is about 6, 6, and 2 times better compared to the localization spots on a metal nanodisk (see Section 4), a nano-crescent-moon (if the same size of the crescent wedge is applied) [21, 22] and a dipole plasmonic nano-antenna [24], respectively. On the other hand, this strong intensity in our RNFA is obtained at only a single spot. Other

#107134 - $15.00 USD Received 3 Feb 2009; revised 3 Mar 2009; accepted 9 Mar 2009; published 11 Mar 2009

structures reported in literatures have multiple localization spots, e.g. a dipole plasmonic antenna has two localized spot at its two ends or a nano-disk results in at least two-spots. This obtained functionality is important for applications like sub-diffraction limited confocal microscopy.

3. Integration of plasmonics with Si photonics

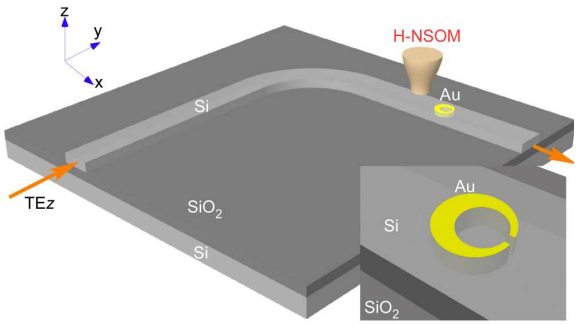

Fig. 2. The proposed realization of the experimental setup consisting of monolithically integrated single gold RNFA, placed at the center of a 1 μm-wide Γ-shaped Si waveguide fabricated using SOI technology.

Our experimental apparatus consists of a lossless Si waveguide integrated with the gold RNFA nanostructure to deliver TE_z-like electromagnetic wave (*x*-polarized light becomes *y*-polarized after the bending area of the waveguide) to the RNFA and excite the LSPs (see Fig. 2). To our knowledge, this is the first integration of Si dielectric waveguide with single localized plasmonic element,, and this integration provides interconnection to and from the nanoantenna, enabling unique plasmonic features (like strong field focusing on nanoscale) that are currently unprecedented in conventional Si photonics. The experiments are designed for operation in the near infrared telecommunication optical spectrum range (~1550 nm). Top faces of the RNFA and waveguide are leveled to efficiently excite resonant LSP around the RNFA as well as easily detect the generated LSP outside the Si waveguide using heterodyne near-field scanning optical microscope (H-NSOM) [26] (see insets of Fig. 2).

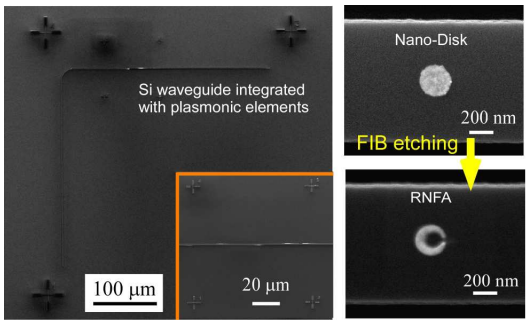

Fig. 3. SEM micrographs of the fabricated monolithically integrated experimental system, including a Si waveguide integrated with a plasmonic RNFA. The FIB technique was used to fabricate the small off-centre cylindrical cut-out and the small gap of RNFA from a nano-disk.

The RNFA sample was fabricated using standard E-beam lithography procedure followed by reactive ion beam etching, gold deposition and focused-ion-beam processing. An SOI wafer with a Si slab thickness of 250 nm and an oxide layer thickness of 3 μm was used to construct the experiment. The Si waveguide was fabricated using the standard E-beam lithography procedure. First, as shown in Fig.3, the designed Si waveguide was fabricated with four alignment marks using the standard E-beam lithography procedure followed by

#107134 - $15.00 USD Received 3 Feb 2009; revised 3 Mar 2009; accepted 9 Mar 2009; published 11 Mar 2009

reactive ion etching (RIE) with Chlorine based chemistry. The second lithography step in fabricating the nano-disks involves spin-coating a 200 nm polymethyl methacrylate (PMMA) onto the entire sample. After the accurate E-beam alignment using the four marks in the Raith50 E-beam Writer, a 250 nm-diameter hole was created in the PMMA mask on the top of the Si waveguide. Chlorine based RIE etching was performed again to etch a 50nm-high cylindrical void in the Si waveguide with PMMA acting as the RIE mask. This cylindrical void was then filled by gold deposition to form the designed gold nano-disk in the Si waveguide. The last fabrication step was performed by using a focused-ion-beam (strata FIB 201, FEI company, 30 keV Ga ions) to make an off-axis cylindrical cut-out and a gap with flat wedges based on the fabricated nanodisk. Finally, the RNFA has been fabricated and placed at the center of a 1 μm-wide Γ-shaped Si waveguide. The diameter and thickness of RNFA are 250 nm and 50 nm, respectively. The center of the 130 nm-diameter cylindrical cut-out is offset from the center of the nano-disk by 40 nm and the gap in the RNFA is only 25 nm (see Fig. 5(a)).

4. Numerical analysis

Finite element computer simulations with commercial software (Ansoft HFSS v9.0) summarized in Fig. 4 are used first to validate our proposed concepts. A comparison between the calculated resonant responses of the electric field intensity (squared magnitude) averaged over the volume defined by half-intensity of the corresponding maximum, which is achieved at the RNFA gap and the LSP localization spots in a simple gold nano-disk, clearly shows about six times resonant enhancement (see Fig. 4(a)). Also notice that the averaged intensity in the RNFA gap is enhanced ~2-order of magnitude compared to light inside the Si waveguide.

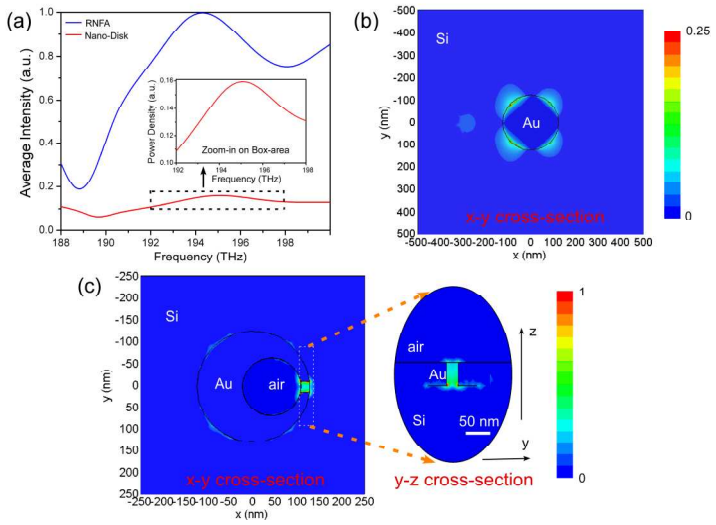

Fig. 4. Comparative numerical analysis of LSP resonance on RNFA and nano-disk: (a) The blue and the red curves show the spectra of the average intensities at the gap of the RNFA nanostructure and the field localization regions of the nano-disk, respectively. (b) Map of the LSP electric field intensity distribution on the top surface of the waveguide and nano-disk interface at the resonant frequency of 195 THz (wavelength of 1538.5 nm). c. Map of the electric field intensity distribution around the RNFA-Si interface (left) and the transverse plane cross-section at the center of the gap of the RNFA structure (right) at the resonant frequency of 194.5 THz (wavelength of 1542 nm).

At the resonant frequency, the LSP field is strongly confined at the edge of the nano-disk and decays exponentially. While in Fig. 4(c), the field is strongly and uniformly localized inside the nano-capacitor formed by the gap with the spot size of about 25 nm along the *x* direction. Note that the RNFA and nano-disk structures share similar eigen-frequencies and

#107134 - $15.00 USD Received 3 Feb 2009; revised 3 Mar 2009; accepted 9 Mar 2009; published 11 Mar 2009

have resemblance in the spatial modal structure. The eigen-frequencies of the LSPs of the two structures are 194.5 THz (wavelength of 1542 nm) for the RNFA and 195 THz (wavelength of 1538.5 nm) for the nano-disk, respectively. The resonant field distributions in Fig. 4(b) and 4(c) also have similar spatial modal structure consisting of four similar peaks along the circular perimeter corresponding to twice the surface plasmon wavelengths length of the resonator round loop. These similarities between the eigen-states have the same nature as the current distribution in a microwave dipole wire antenna, which is nearly identical to the case of free standing wire and an antenna of the same size fed through a small gap. Due to reciprocity, which is one of the fundamental principles of electromagnetism, the gap does not change significantly the source-excited or source-free field/current distributions as well as eigen-frequencies of such structures.

In other words, the LSP resonance in RNFA can be seen as a "short-circuit" resonance compared to the LSP resonance in nano-disks. The definition of "short- and open-circuit" resonances is given in Ref. 25. The "short-circuit" resonance corresponds to the case where the small gap (the capacitor) is located at the minimum of the electric field in the original nano-disk. Without a gap, the magnetic field is the strongest and the electric field is the weakest at this location (hence the notation "short-circuit"). With the gap placed at this "short-circuit" location, the time variations of the strong magnetic field lead to a voltage in the gap. The presence of this voltage, however, does not affect significantly the modal field because the gap is small and this effect is local. However, since the gap is small the voltage is transformed into a very strong local electric field between the gap edges just like in a capacitor. As mentioned above, this behavior is of the same nature as in the feed points of many gap fed microwave antennas, e.g. dipole antennas. The optical field impedance values of thin metallic wedges and the small gap associated with this "short-circuit" resonance are close to zero. Thus the impedance value of the entire RNFA geometry is similar to its original nano-disk's [25].

For the open-circuit case, the situation is opposite, i.e. the modal magnetic field is minimal at the gap location. Therefore, the resulting electric field in the gap is weak. The modal electric field still has a maximum, which however is much lower than the strong field enhancement obtained due to the gap field localization.

With the "short-circuit" resonance, the fact that resonant frequencies of the nano-disk and RNFA are close has an important practical implication in relaxing the fabrication tolerance for constructing the RNFA from a nano-disk. Moreover, for the complicated RNFA structure, its eigen-frequencies can be characterized by developing closed form approximate expressions for a simple nano-disk structure. While the LSP field impedance and resonant frequencies do not change, the presence of the sharp thin metallic wedges and the small gap results in more than 6-fold enhancement of the field intensity (see Fig. 4(a)) localized in all 3 dimensions inside the nano-capacitor with a 25 nm gap.

5. Experimental characterizations

The near field H-NSOM measurements are performed first with a tip scanning step size of 100 nm to locate the resonance by simultaneously scanning the optical frequencies of the input field in the range of 191 THz to 196 THz over a scanning area of 15 μm × 15 μm centered on the RNFA. The data shows a strong LSP localization at the frequency of 194.2 THz (λ_0=1544.9 nm).

The waveguide mode was successfully converted to the highly confined LSP resonance mode in the RNFA (see Fig. 5(b)). We can see here that the introduction of our RNFA does not strongly disturb the original waveguide mode as the transmission of the light in the waveguide after RNFA is about 65%, since the height and the size of RNFA are significantly smaller than the waveguide size and the modal extent. Next we use the input optical field at the resonant frequency to detect a high resolution near field intensity map with H-NSOM tip scanning step size of 10 nm (see Fig. 5(c)). The strong field localization obtained experimentally in Fig. 5(c) corresponds to the resonance of LSPs on the RNFA. The measured

#107134 - $15.00 USD Received 3 Feb 2009; revised 3 Mar 2009; accepted 9 Mar 2009; published 11 Mar 2009

spot size along the x direction taking into account the finite probe aperture size was about 220 nm. Since the expected nanofocusing spot size is only tens of nanometres (corresponding to the size of the nano-capacitor), the measurement of the actual size even with current H-NSOM techniques [26] is challenging owing to the size and the electromagnetic interaction between the probe and the measured structure. We consider these near field interaction effects in the RNFA characterization experiments by including a deconvolution procedure into our H-NSOM process (see Appendix). In the a restored near field intensity image shown in Fig. 5(d), the estimated effect of the probe on the convolution with the measured localized optical field is an effective aperture of about 155±5 nm, consistent with the estimates achieved for other plasmonic nanostructures we tested in H-NSOM measurement (e.g. 150 nm for nanodisks). An elliptical focusing spot was obtained, which is associated with a slightly weaker localization in the y direction. The field localization along the x direction estimated from the restored measured data in Fig. 5(d) is about 75±5 nm.

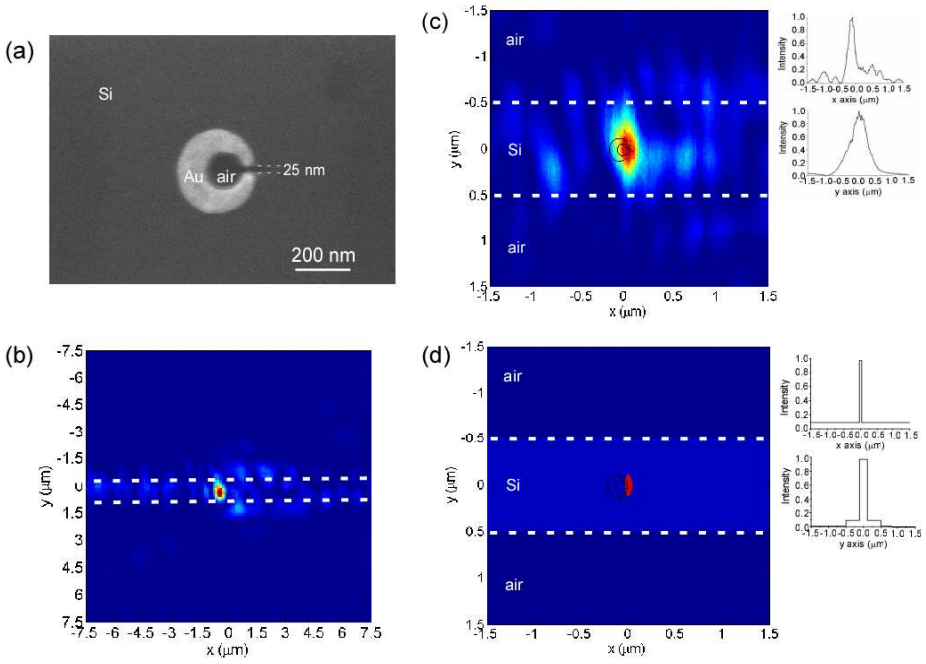

Fig. 5. Experimental results on characterization of the optical field localization in resonant RNFA geometry. (a) SEM micrograph of the RNFA geometry. (b) Low resolution H-NSOM field intensity at the frequency of 194.2THz (wavelength of 1544.9 nm). The bright spot in the middle of the waveguide (see dotted line) corresponds to the highly confined LSP modes in RNFA. (c) Raw H-NSOM image of high resolution intensity mapping measured at 194.2 THz. (d) Processed image of the field intensity in the same area after deconvolution signal processing to extract the effect of the NSOM probe on the measured data. Insets of (c) and (d) show the cross-section data along the *x* (top) and *y* (bottom) axis. The RNFA shaped sketch in (c) and (d) indicates the position of the RNFA geometry. .

As shown in Fig. 4a, the Quality factor of our RNFA is determined by the original nano-disk and is typically about 10. Thus the intensity as well as field distribution varies relatively slowly with different wavelengths. This means that, within the range we did the simulation and measurement, the field distribution on the structure is very similar (strong focusing spot in the gap and other 4 bright spots on the sidewall can be obtained) but the coupling efficiency is slightly lower for off-resonant excitation. For example, at the wavelength of 192.3 THz (λ_0=1560 nm) the measurement results show that the contrast of the focusing spot to the incident waveguide mode is about twice lower than that under the resonant excitation in Fig. 5(c).

#107134 - $15.00 USD Received 3 Feb 2009; revised 3 Mar 2009; accepted 9 Mar 2009; published 11 Mar 2009

6. Summary

The RNFA geometry has been analyzed theoretically and demonstrated experimentally to efficiently convert a waveguide mode into a resonant LSP mode, which is localized into an extraordinary small volume of deeply subwavelength size in nanoscale. In principle, the size of the localization is only determined by the size of the RNFA's gap. Such strong field localization is obtained due to combined effects of the resonant LSPs, edge localization by the sharp thin metallic wedges, and TEM field localization in the gap nano-capacitor. The presented structure and phenomena are anticipated to have important impacts on many applications including constructing novel devices for bio-medical imaging, bio-sensing, nano-lithography, heat-assisted magnetic recording, and plasmonic nanocircuits operating at optical frequencies. In addition, our integration of conventional Si photonics (e. g., Si waveguides) with plasmonic elements will also help to further advance incorporating unique unprecedented functionalities enabled by plasmonic devices into Si photonics.

Appendix

Deconvolution procedure

Once the aperture of H-NSOM's probe is comparable or bigger than the size of the localized optical field, the experimentally measured spot size is affected by the tip size and its interference with the plasmonic nanostructure. To estimate the size of the plasmonic localization, we need to perform measured data post-processing.

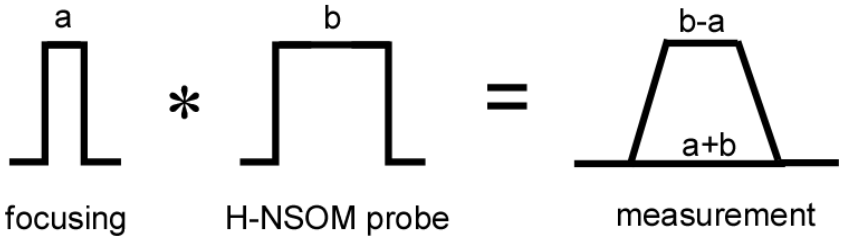

Fig. A1. Description of the digital post-processing deconvolution process to estimate the size of the localized field spot size from the measured data.

For simplicity, we consider a 1-dimensional case and make an assumption that the impulse response functions for both the localized field being characterized and the probe aperture of the H-NSOM have shapes of $\mathrm{rect}(x/a)$ and $\mathrm{rect}(x/b)$ functions with their corresponding widths of a and b, respectively. The result of the convolution between such two rectangular functions produces a trapezoid shape (see Fig. A1), representing an approximation to the measured data. The widths of this trapezoid's bases are $b-a$ and $a+b$, respectively, and both of them can be retrieved from the measured data obtained in the experiments. Hence, the actual focusing and the probe effect can be retrieved once the trapezoid shape is established.

To find the trapezoid shape from the measured data (see Fig. 5(c)), we first perform a Gaussian fit with minimum variance. The intuition of the Gaussian fitting can be viewed as first finding a Gaussian-shaped bounded stripe area that tightly wraps the data inside and then choose the center contour of this stripe as the fitting result. Hence, it should be statistically reasonable to take the peak value as the average of the data within the central region [27]. The peak value of the Gaussian fit was thus chosen as the upper base of the trapezoid. The linear fit was performed twice on the Gaussian curve separately, before and after the peak, to obtain two sides of the trapezoid. Fig. A2 shows the raw data along the *x* direction (extracted from Fig. 5(c)) and the corresponding trapezoidal fits with minimum variance for the RNFA.

#107134 - $15.00 USD Received 3 Feb 2009; revised 3 Mar 2009; accepted 9 Mar 2009; published 11 Mar 2009

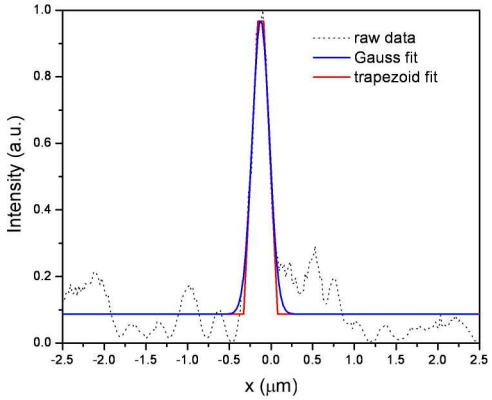

Fig. A2. Intensity distributions of the measured experimental data along the *x* direction determined from Fig. 5(c) for RNFA. A trapezoidal fit (red) is performed to a Gaussian fit (blue) of the measured data (black dotted).

This trapezoidal fit was performed 4 times for measured data from Fig. 5(c) along the *x*, *y*, *xy* and *–xy* directions. The 1-dimensional estimates along these directions are used to approximate the 2-dimensional field in the x-y plane similar to that in Fig. 5(c). The retrieved widths of the localized field spot sizes from these 4 trapezoids along the 4 directions corresponding directions were used to create a fit by an ellipse in *x*-*y* plane using minimum variance criterion.

We call this procedure deconvolution process. The resulting ellipse represents the estimated restored local field spot size and is used to calculate the fields in Figs. 5(d).

Acknowledgment

This work is supported by DARPA Center for Optofluidic Integration and NSF.

#107134 - $15.00 USD Received 3 Feb 2009; revised 3 Mar 2009; accepted 9 Mar 2009; published 11 Mar 2009